The liquid-gas phase transition and the caloric curve of nuclear matter

K. Miyazaki

E-mail: miyazakiro@rio.odn.ne.jp

Abstract

A new relativistic mean-field model, which reproduces the astronomical observations of neutron stars and the experimental nuclear symmetry energy, is applied to warm nuclear matter. We confirm that the model also reproduces the critical temperature and the caloric curve in the liquid-gas phase transition of nuclear matter.

The recent great experimental progress [1-4] in nuclear multifragmentation reaction has revealed the liquid-gas phase transition of nuclear matter. Its signals are observed in the critical phenomena [5-8], the caloric curve [9,10], the negative heat capacity [11,12] and the bimodality [13]. The phase transition provides valuable information on nuclear equation of state (EOS) at sub-saturation densities. On the other hand, the recent astronomical observations of neutron stars (NSs) provide the information on the EOS at super-saturation densities. In the theoretical point of view it is desirable to reproduce both the EOSs of dilute and dense nuclear matter and both the EOSs of warm and cool nuclear matter simultaneously on the single fundamental model of nuclear system.

It has been found recently [14,15] that the reasonable description of NS matter requires the relativistic mean-field (RMF) model, which takes into account the field-dependent meson-nucleon coupling constants. In this respect, we have developed a new RMF model [16], which reproduces the mass-radius relation of NS [17] and satisfies the standard scenario of NS cooling. Moreover, the model reproduces the density-dependence of nuclear symmetry energy [18-20] at sub-saturation densities. It is therefore worthwhile to investigate the applicability of the model to the liquid-gas phase transition of warm nuclear matter.

In Ref. [16] we have introduced the modified scalar and vector vertices of isoscalar meson:

$$\begin{aligned} I \;\rightarrow\; & \left[\Lambda^{(+)}(p')\, I\, \Lambda^{(+)}(p) + \Lambda^{(-)}(p')\, I\, \Lambda^{(-)}(p)\right] \\ & + \lambda_\sigma \left[\Lambda^{(+)}(p')\, I\, \Lambda^{(-)}(p) + \Lambda^{(-)}(p')\, I\, \Lambda^{(+)}(p)\right] \\ = \;& \frac{(1-\lambda_\sigma)\, \not{p}'\, \not{p} + (1+\lambda_\sigma)\, M_N^2}{2\, M_N^2}, \end{aligned} \tag{1}$$

$$\begin{aligned}\gamma^{\mu} &\rightarrow \lambda_{\omega}\left[\Lambda^{(+)}\left(p'\right)\gamma^{\mu}\Lambda^{(+)}\left(p\right)+\Lambda^{(-)}\left(p'\right)\gamma^{\mu}\Lambda^{(-)}\left(p\right)\right] \\ &\quad +\left[\Lambda^{(+)}\left(p'\right)\gamma^{\mu}\Lambda^{(-)}\left(p\right)+\Lambda^{(-)}\left(p'\right)\gamma^{\mu}\Lambda^{(+)}\left(p\right)\right] \\ &= \frac{\left(\lambda_{\omega}-1\right)\not{p}'\gamma^{\mu}\not{p}+\left(\lambda_{\omega}+1\right)M_N^2\gamma^{\mu}}{2\,M_N^2}, \end{aligned} \tag{2}$$

where $\Lambda^{(\pm)}$ is the positive (negative) energy projection operator for the Dirac nucleon of mass M_N,

$$\Lambda^{(\pm)}\left(p\right)=\frac{\pm\not{p}+M_N}{2\,M_N}. \tag{3}$$

The modified vertices for the isovector mesons have been also defined similarly. They are reduced to the field-dependent effective NNX ($X=\sigma$, ω, δ and ρ) coupling constants.

$$g^{*}_{pp(nn)X}=\frac{1}{2}\left[\left(1+\lambda_X\right)+\left(1-\lambda_X\right)\left(\left(m^{*}_{p(n)}\right)^2-v^2_{p(n)}\right)\right]g_{NNX}. \tag{4}$$

In the RMF theory the Lagrangian for asymmetric nuclear matter is

$$\begin{aligned}\mathcal{L} &= \bar{\psi}_p\left(\not{p}-\gamma^0\,V_p-M^{*}_p\right)\psi_p+\bar{\psi}_n\left(\not{p}-\gamma^0\,V_n-M^{*}_n\right)\psi_n \\ &\quad -\frac{1}{2}\,m^2_{\sigma}\left\langle\sigma\right\rangle^2+\frac{1}{2}\,m^2_{\omega}\left\langle\omega_0\right\rangle^2-\frac{1}{2}\,m^2_{\delta}\left\langle\delta_3\right\rangle^2+\frac{1}{2}\,m^2_{\rho}\left\langle\rho_{03}\right\rangle^2, \end{aligned} \tag{5}$$

where ψ_p and ψ_n are the Dirac fields of proton and neutron. We have taken into account the isovector-scalar meson δ besides the isovector-vector meson ρ. $M^{*}_i=m^{*}_iM_N=M_N+S_i$ is the effective mass of a proton or a neutron in the medium. The scalar and vector potentials are given by

$$S_p=-g^{*}_{pp\,\sigma}\left\langle\sigma\right\rangle-g^{*}_{pp\delta}\left\langle\delta_3\right\rangle, \tag{6}$$

$$S_n=-g^{*}_{nn\sigma}\left\langle\sigma\right\rangle+g^{*}_{nn\delta}\left\langle\delta_3\right\rangle, \tag{7}$$

$$V_p=g^{*}_{pp\,\omega}\left\langle\omega_0\right\rangle+g^{*}_{pp\rho}\left\langle\rho_{03}\right\rangle, \tag{8}$$

$$V_n=g^{*}_{nn\,\omega}\left\langle\omega_0\right\rangle-g^{*}_{nn\rho}\left\langle\rho_{03}\right\rangle. \tag{9}$$

We assume $\lambda_{\sigma}=\lambda_{\omega}=\lambda_0$ and $\lambda_{\delta}=\lambda_{\rho}=\lambda_1$ in Eq. (4). The value $\lambda_0=2/3$ is determined [16] so as to reproduce $m^{*}_p=m^{*}_n\simeq 0.6$ in the saturated symmetric nuclear matter. The parameter λ_1 is constrained within the range $0\leq\lambda_1\leq 0.2$ [16] so that the direct URCA cooling is forbidden in NSs. In the present work we assume a value $\lambda_1=0$, which reproduces the nuclear symmetry energy $E_{sym}\left(\rho\right)=31.6\left(\rho/\rho_0\right)^{0.7}$ being consistent with the experimental analyses in Refs. [18-20].

At finite temperature T the thermodynamic potential per volume $\tilde{\Omega}\equiv\Omega/V$ of asym-

metric nuclear matter is

$$\begin{aligned}\tilde{\Omega} &= \frac{1}{2}\,m_\sigma^2\,\langle\sigma\rangle^2 + \frac{1}{2}\,m_\delta^2\,\langle\delta_3\rangle^2 - \frac{1}{2}\,m_\omega^2\,\langle\omega_0\rangle^2 - \frac{1}{2}\,m_\rho^2\,\langle\rho_{03}\rangle^2 \\ &- \gamma\,k_B\,T\sum_{i=p,n}\int_0^\infty \frac{d^3\mathbf{k}}{(2\,\pi)^3}\left\{\ln\left[1+\exp\left(\frac{\nu_i - E_{ki}^*}{k_B\,T}\right)\right] + \ln\left[1+\exp\left(\frac{-\nu_i - E_{ki}^*}{k_B\,T}\right)\right]\right\},\end{aligned} \tag{10}$$

where k_B is the Boltzmann constant and $E_{ki}^* = (\mathbf{k}^2 + M_i^{*2})^{1/2}$. The spin-isospin degeneracy γ is equal to 2. The ν_i is defined using the chemical potential μ_i and the vector potential V_i of a proton or a neutron:

$$\nu_i = \mu_i - V_i. \tag{11}$$

The effective masses $M_i^* = m_i^* M_N$ and the vector potentials $V_i = v_i M_N$ are determined by extremizing $\tilde{\Omega}$:

$$\begin{aligned}\frac{\partial\,\tilde{\Omega}}{\partial\,V_{p(n)}} &= \rho_{p(n)} + m_\sigma^2\,\frac{\langle\sigma\rangle}{M}\,\frac{\partial\,\langle\sigma\rangle}{\partial\,v_{p(n)}} + m_\delta^2\,\frac{\langle\delta_3\rangle}{M}\,\frac{\partial\,\langle\delta_3\rangle}{\partial\,v_{p(n)}} \\ &- m_\omega^2\,\frac{\langle\omega_0\rangle}{M}\,\frac{\partial\,\langle\omega_0\rangle}{\partial\,v_{p(n)}} - m_\rho^2\,\frac{\langle\rho_{03}\rangle}{M}\,\frac{\partial\,\langle\rho_{03}\rangle}{\partial\,v_{p(n)}} \;=\; 0,\end{aligned} \tag{12}$$

$$\begin{aligned}\frac{\partial\,\tilde{\Omega}}{\partial M_{p(n)}^*} &= \rho_{Sp(n)} + m_\sigma^2\,\frac{\langle\sigma\rangle}{M}\,\frac{\partial\,\langle\sigma\rangle}{\partial\,m_{p(n)}^*} + m_\delta^2\,\frac{\langle\delta_3\rangle}{M}\,\frac{\partial\,\langle\delta_3\rangle}{\partial\,m_{p(n)}^*} \\ &- m_\omega^2\,\frac{\langle\omega_0\rangle}{M}\,\frac{\partial\,\langle\omega_0\rangle}{\partial\,m_{p(n)}^*} - m_\rho^2\,\frac{\langle\rho_{03}\rangle}{M}\,\frac{\partial\,\langle\rho_{03}\rangle}{\partial\,m_{p(n)}^*} \;=\; 0,\end{aligned} \tag{13}$$

where the mean-fields are calculated from the effective masses and the vector potentials. See Eqs. (42)-(47) in Ref. [16]. The explicit expressions of the derivatives of mean fields are also given in Ref. [16]. The baryon and scalar densities are defined by

$$\rho_{Bi} = \gamma\int_0^\infty \frac{d^3\mathbf{k}}{(2\,\pi)^3}\,[\,n_{ki}\,(\mu_i, T) - \bar{n}_{ki}\,(\mu_i, T)], \tag{14}$$

$$\rho_{Si} = \gamma\int_0^\infty \frac{d^3\mathbf{k}}{(2\,\pi)^3}\,\frac{M_i^*}{E_{ki}^*}\,[\,n_{ki}\,(\mu_i, T) + \bar{n}_{ki}\,(\mu_i, T)]. \tag{15}$$

The Fermi-Dirac distribution functions of nucleon and antinucleon are

$$n_{ki}\,(\mu_i, T) = \left[1 + \exp\left(\frac{E_{ki}^* - \nu_i}{k_B\,T}\right)\right]^{-1}, \tag{16}$$

$$\bar{n}_{ki}\left(\mu_i, T\right) = \left[1 + \exp\left(\frac{E^*_{ki} + \nu_i}{k_B\, T}\right)\right]^{-1}. \tag{17}$$

The pressure is given by

$$\begin{aligned} P &= \frac{1}{3\,\pi^2} \sum_{i=p,n} \int_0^\infty dk\, \frac{k^4}{E^*_{ki}} \left[\, n_{ki}\left(\mu_i, T\right) + \bar{n}_{ki}\left(\mu_i, T\right)\right] \\ &\quad - \frac{1}{2}\, m_\sigma^2 \left\langle\sigma\right\rangle^2 - \frac{1}{2}\, m_\delta^2 \left\langle\delta_3\right\rangle^2 + \frac{1}{2}\, m_\omega^2 \left\langle\omega_0\right\rangle^2 + \frac{1}{2}\, m_\rho^2 \left\langle\rho_{03}\right\rangle^2. \end{aligned} \tag{18}$$

In the following calculations we have performed the Fermi integral directly using the adaptive automatic integration with 20-points Gaussian quadratures.

Given the temperature T and the total baryon density

$$\rho_B = \rho_{Bp} + \rho_{Bn}, \tag{19}$$

we can solve the 3rd-rank nonlinear simultaneous equations (12), (13) and (19) using the Newton-Raphson method so that we have the effective mass $m^*_p = m^*_n$, the vector potential $v_p = v_n$ and the chemical potential $\mu_p = \mu_n$ of a nucleon in symmetric nuclear matter. Figure 1 shows the isotherms in the pressure-density plane for symmetric nuclear matter. (In the following we set $k_B = 1$.) They exhibit typical nature of van der Waals EOS, that is, the liquid-gas phase transition. $T = 12.95$MeV is the flash temperature above which the pressure is always positive at any density. We have found the critical temperature $T_C = 16.47$MeV, where the isotherm has an inflection point at $P_C = 0.3176\text{MeV/fm}^3$ and $\rho_C = 0.06\text{fm}^{-3}$. The result agrees well with the empirical value $T_C = 16.6 \pm 0.86$MeV in Ref. [21].

For asymmetric nuclear matter, given the temperature, the baryon density and the isospin asymmetry a

$$a = \frac{\rho_{Bn} - \rho_{Bp}}{\rho_B}, \tag{20}$$

we solve the 6th-rank nonlinear simultaneous equations (12), (13), (19) and (20) so that we have the effective masses m^*_p and m^*_n, the vector potentials v_p and v_n and the chemical potentials μ_p and μ_n of proton and neutron. Figure 2 shows the isotherms for $a = 0.3$. They are also similar to the van der Waals EOS. The flash temperature is $T = 11.84$MeV. The critical temperature is $T = 15.26$MeV. The critical point lies at $P_C = 0.2875\text{MeV/fm}^3$ and $\rho_C = 0.059\text{fm}^{-3}$. Although the critical density is insensitive to the asymmetry, the critical temperature and pressure decrease as the asymmetry increases.

Next, we investigate asymmetric nuclear matter under constant pressure. It would be produced in nuclear multifragmentation reaction. In this case we have to solve 7th-rank nonlinear simultaneous equations (12), (13), (18), (19) and (20) so that the effective masses m^*_p and m^*_n, the vector potentials v_p and v_n, the chemical potentials μ_p and μ_n

and the temperature T are determined. The quantity characterizing the thermodynamic process under constant pressure is the enthalpy H:

$$\tilde{H} = H/V = \mathcal{E} + P, \tag{21}$$

where the energy density is given by

$$\begin{aligned} \mathcal{E} &= \sum_{i=p,n} \left\{ \int_0^\infty \frac{d^3\mathbf{k}}{(2\,\pi)^3} E^*_{ki} \left[n_{ki}\left(\mu_i, T\right) + \bar{n}_{ki}\left(\mu_i, T\right) \right] + V_i\, \rho_{Bi} \right\} \\ &\quad + \frac{1}{2}\, m_\sigma^2 \left\langle \sigma \right\rangle^2 + \frac{1}{2}\, m_\delta^2 \left\langle \delta_3 \right\rangle^2 - \frac{1}{2}\, m_\omega^2 \left\langle \omega_0 \right\rangle^2 - \frac{1}{2}\, m_\rho^2 \left\langle \rho_{03} \right\rangle^2 . \end{aligned} \tag{22}$$

The entropy $\tilde{S} = S/V$ is calculated in terms of the Gibbs-Duhem relation $T\tilde{S} = \tilde{H} - \tilde{G}$, where $\tilde{G} = G/V = \mu_p \rho_{Bp} + \mu_n \rho_{Bn}$ is the Gibbs energy per volume.

We have calculated the asymmetric nuclear matter of an asymmetry $a = 0.3$ under a constant pressure $P = 0.025\text{MeV/fm}^3$. Figure 3 shows the entropy per particle $S/A = \tilde{S}/\rho_B$ as a function of the enthalpy per particle $H/A = \tilde{H}/\rho_B$. Our numerical result, the black curve, has a dip or a convex intruder between H/A =3.4MeV and 30.7MeV as a result of the liquid-gas phase transition. Because the entropy should be concave, the convex intruder is not realized but the common tangent depicted by the red line is realized according to the principle of increasing entropy. Because of $\partial S/\partial H = 1/T$ we can determine the boiling temperature $T = 7.91$MeV of nuclear liquid from the inclination of the common tangent. The value is also determined more directly from an intersection in the T-$\tilde{G}$ plain.

The black curve in Fig. 4 shows the caloric curve, the temperature as a function of the excitation energy per particle. The dotted part corresponds to the convex intruder of the entropy in Fig. 3 and so is replaced by the horizontal line of the boiling temperature $T = 7.91$MeV. The triangles are the experimental data from the multifragmentation reaction of Fig. 5 in Ref. [10]. Although the black curve does not agree well with the data at low excitation energies, the plateau, which corresponds to the metastable liquid-gas mixed phase, is reproduced.

We note in Fig. 4 that the last experimental datum lies above the boiling temperature. It may be a signal that the liquid-gas phase becomes unstable. The thermodynamic conditions of the (meta-)stable state are

$$\frac{\partial P}{\partial \rho_B} \geq 0, \tag{23}$$

$$\frac{T}{C_p} = \frac{\partial T}{\partial S} \geq 0. \tag{24}$$

The first condition determines the spinodal region. Its boundary is depicted by the red dotted curve in Fig. 2. The boundary for $P = 0.025\text{MeV/fm}^3$ is $\rho_B = 0.086\text{fm}^{-3}$. The

corresponding excitation energy is $E^*/A = 11.87$MeV. The boundary of the second condition is just on the extreme of temperature shown by the red vertical line in Fig. 4. We have $T = 12.11$MeV at $E^*/A = 11.86$MeV. Both the conditions (23) and (24) agree with each other. Above the boiling temperature the caloric curve would be described [22] by $E^*/A = (3/2)\,T$ of a free gas. It is shown by the blue dashed line in Fig. 4. For $T = 7.91$MeV we have $E^*/A = 11.865$MeV. The value agrees fairly well with the thermodynamic conditions (23) and (24). The black line is therefore connected continuously to the blue line.

Finally, we should refer to Ref. [23], which showed that the asymmetric nuclear matter was the binary system with two independent chemical potentials of proton and neutron. Based on the Gibbs condition of phase equilibrium, both the chemical potentials were equilibrated in the liquid-gas mixed phase. The geometrical construction was used to determine them. Such a technique is widely used in the other works [24-26] of the liquid-gas phase transition in asymmetric nuclear matter. To the contrary, in the common tangent method used in the present work, only the Gibbs energy is equilibrated. However, the upper limit on the plateau in the caloric curve of Fig. 4 is likely to support our analysis. Moreover, it is noted that the geometrical construction of the equilibrated chemical potentials is appropriate to the canonical ensemble, in which the chemical potentials are the functions of temperature, while the nuclear matter produced in multifragmentation reaction is the microcanonical ensemble, in which the chemical potentials and the temperature are determined individually for fixed values of the other quantities. In fact, for the caloric curve of Fig. 4 we investigate the microcanonical ensemble of nuclear matter. Now we are planning the physically reasonable calculation of the liquid-gas phase transition in the microcanonical ensemble of the binary nuclear system. It does not rely on the common tangent method nor the geometrical construction.

We have applied the RMF model developed in Ref. [16] to warm asymmetric nuclear matter. The model can reproduce the astronomical observations of NSs and the experimental nuclear symmetry energy, simultaneously. We have found that the model is also useful to the liquid-gas phase transition of nuclear matter. The critical temperature and the caloric curve are reproduced. The latter has been calculated in the microcanonical ensemble. Although we are based on the traditional assumptions of thermodynamics, the concavity and the extensivity of entropy, they are never obvious. In fact, it has been recently reported [11,12] that the entropy of finite nuclei really has a convex intruder and so the negative heat capacity. They are also observed [27-29] in other small finite systems. On the other hand, Ref. [30] analyzed the nuclear multifragmentation in the so-called Tsallis statistics [31,32], which violates the extensivity of entropy. It is an interesting subject to extend our model to finite nuclei in the nonextensive statistics.

References

[1] J. Richert and P. Wagner, Phys. Rep. **350** (2001) 1 [arXiv:nucl-th/0009023].

[2] S.D. Gupta, A.Z. Mekjian and M.B. Tsang, *Advances in Nuclear Physics*, Vol. **26** (Kluwer Academic, 2001) [arXiv:nucl-th/0009033].

[3] V.E. Viola *et al.*, Phys. Rep. **434** (2006) 1 [arXiv:nucl-ex/0604012].

[4] V.A. Karnaukhov, Phys. Elem. Part. Atom. Nucl. **37** (2006) 312 on http://www1.jinr.ru/Pepan/Pepan_index.html

[5] B.K. Srivastava *et al.*, Phys. Rev. C **65** (2002) 054617 [arXiv:nucl-ex/0202023].

[6] J.B. Elliott *et al.*, Phys. Rev. C **67** (2003) 024609 [arXiv:nucl-ex/0205004].

[7] D. Kudzia, B. Wilczyńka and H. Wilczyński, Phys. Rev. C **68** (2003) 054903 [arXiv:nucl-ex/0207017].

[8] Y.G. Ma *et al.*, Phys. Rev. C **71** (2005) 054606 [arXiv:nucl-ex/0410018].

[9] J.B. Natowitz *et al.*, Phys. Rev. C **65** (2002) 034618 [arXiv:nucl-ex/0106016].

[10] A. Ruangma *et al.*, Phys. Rev. C **66** (2002) 044603.

[11] M. D'Agostino *et al.*, Phys. Lett. B **473** (2000) 219 [arXiv:nucl-ex/9906004].

[12] B. Borderie *et al.*, Nucl. Phys. A **734** (2004) 495 [arxiv:nucl-ex/0311016].

[13] O. Lopez and M.F. Rivet, Eur. Phys. J. A **30** (2006) 263 [arXiv:nucl-ex/0611014].

[14] T. Klähn *et al.*, arXiv:nucl-th/0602038.

[15] K. Miyazaki, Mathematical Physics Preprint Archive (mp_arc) 06-103.

[16] K. Miyazaki, Mathematical Physics Preprint Archive (mp_arc) 06-336.

[17] F. Őzel, Nature **441** (2006) 1115 [arXiv:astro-ph/0605106].

[18] B-A. Li and L-W. Chen, Phys. Rev. C **72** (2005) 064611 [arXiv:nucl-th/0508024].

[19] Z-H. Li, L-W. Chen, C.M. Ko, B-A. Li and H-R. Ma, Phys. Rev. C **74** (2006) 044613 [arXiv:nucl-th/0606063].

[20] D.V. Shetty, S.J. Yennello and G.A. Souliotis, arXiv:nucl-ex/0610019.

[21] J.B. Natowitz *et al.*, Phys. Rev. Lett. **89** (2002) 212701 [arXiv:nucl-ex/0204015].

[22] C.E. Aguiar, R. Donangelo and S.R. Souza, Phys. Rev. C **73** (2006) 024613.

[23] H. Műller and B. D. Serot, Phys. Rev. C **52** (1995) 2072 [arXiv:nucl-th/9505013].

[24] P.K. Panda, G. Klein, D.P. Menezes and C. Providência, Phys. Rev. C **68** (2003) 015201 [arXiv:nucl-th/0306045].

[25] P. Wang, D.B. Leinweber, A.W. Thomas and A.G. Williams, Nucl. Phys. A **748** (2005) 226 [arXiv:nucl-th/0407057].

[26] J. Xu. L-W. Chen, B-A. Li and H-R. Ma, arXiv:nucl-th/0702085.

[27] M. Schmidt *et al.*, Phys. Rev. Lett. **86** (2001) 1191.

[28] D.H.E. Gross and J.F. Kenney, J. Chem. Phys. **122** (2005) 224111.

[29] C. Junghans, M. Bachmann and W. Janke, Phys. Rev. Lett. **97** (2006) 218103.

[30] K.K. Gudima, A.S. Parvan, M. Płoszajczak and V.D. Toneev, Phys. Rev. Lett. **85** (2000) 4691 [arXiv:nucl-th/0003025].

[31] C. Tsallis, Braz. J. Phys. **29** (1999) 1.

[32] Europhysics News **36** (2005) No.6 [http://www.europhysicsnews.com].

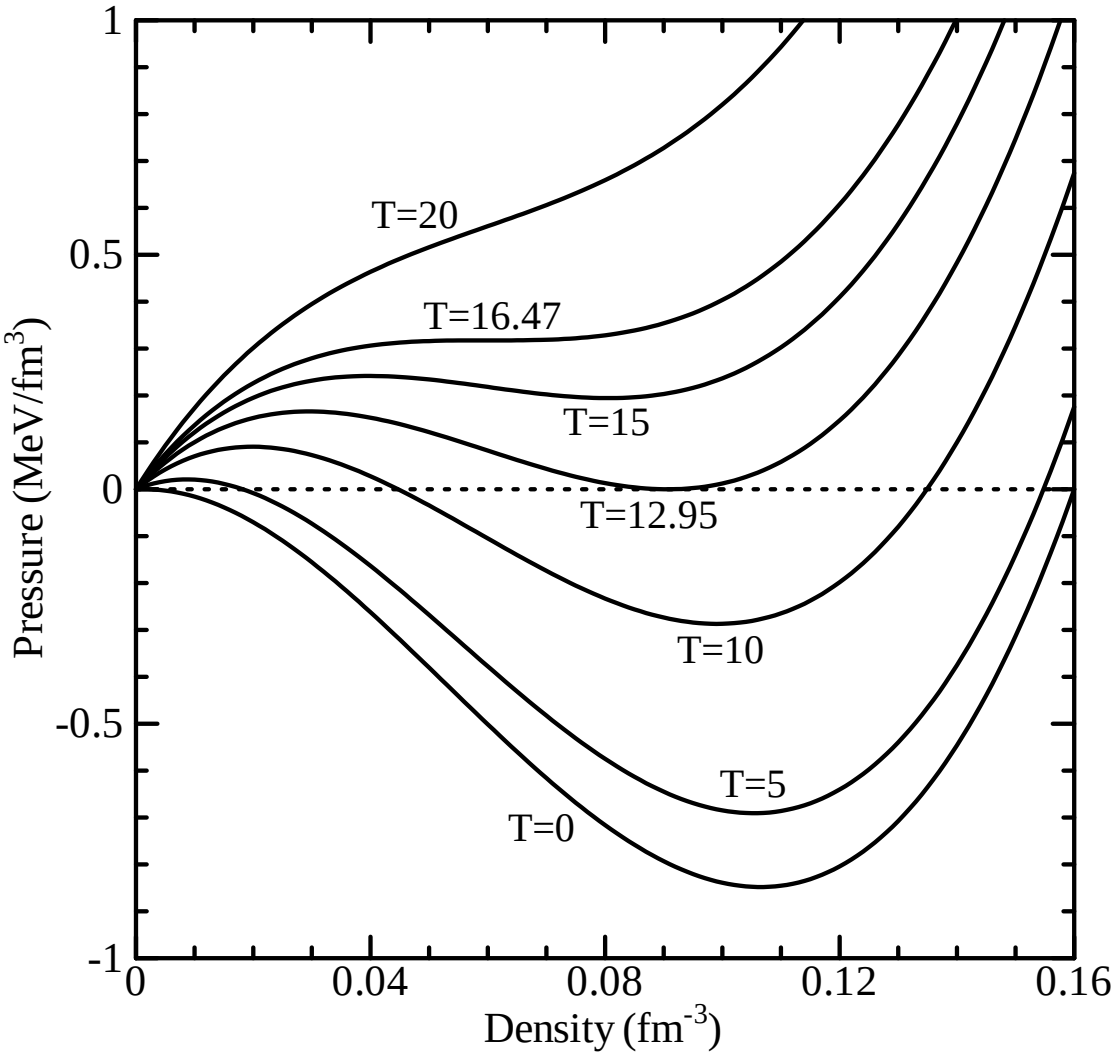

Figure 1: The isotherms in the pressure-density plane for symmetric nuclear matter.

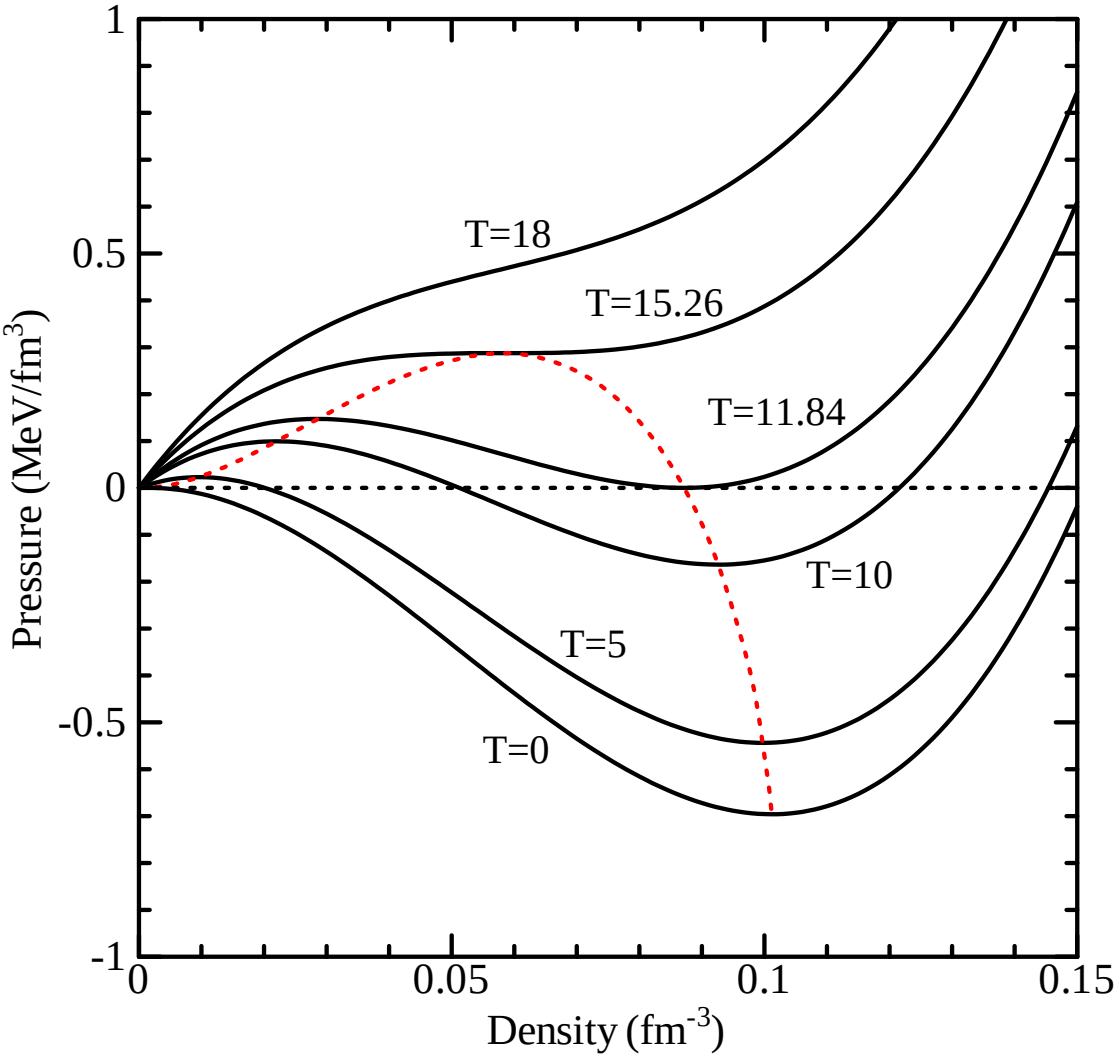

Figure 2: The isotherms in the pressure-density plane for asymmetric nuclear matter of an asymmetry $a = 0.3$. The red dotted curve shows the spinodal boundary.

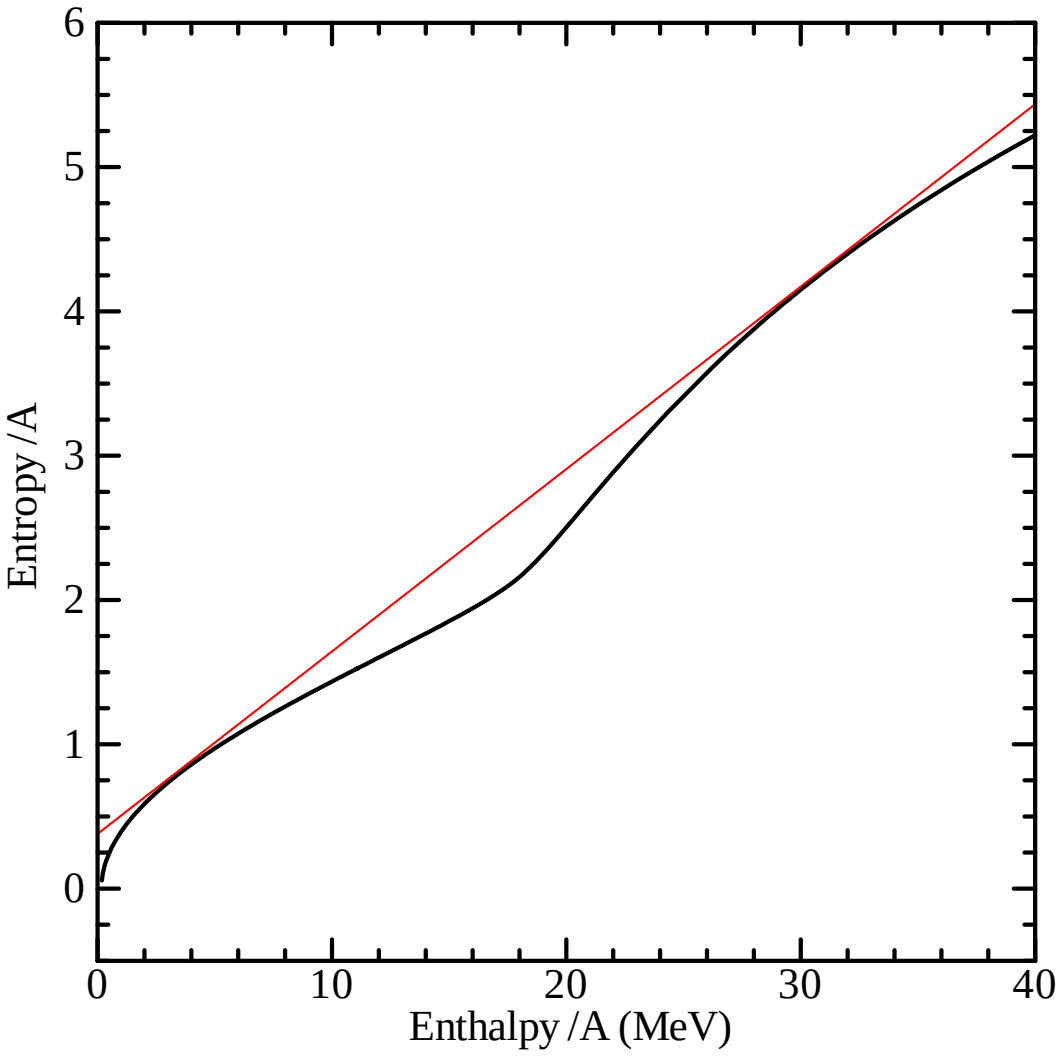

Figure 3: The black curve is the entropy per particle as a function of the enthalpy per particle for asymmetric nuclear matter of an asymmetry $a = 0.3$ under a constant pressure $P = 0.025\mathrm{MeV/fm}^3$. The red line shows the common tangent of the black curve.

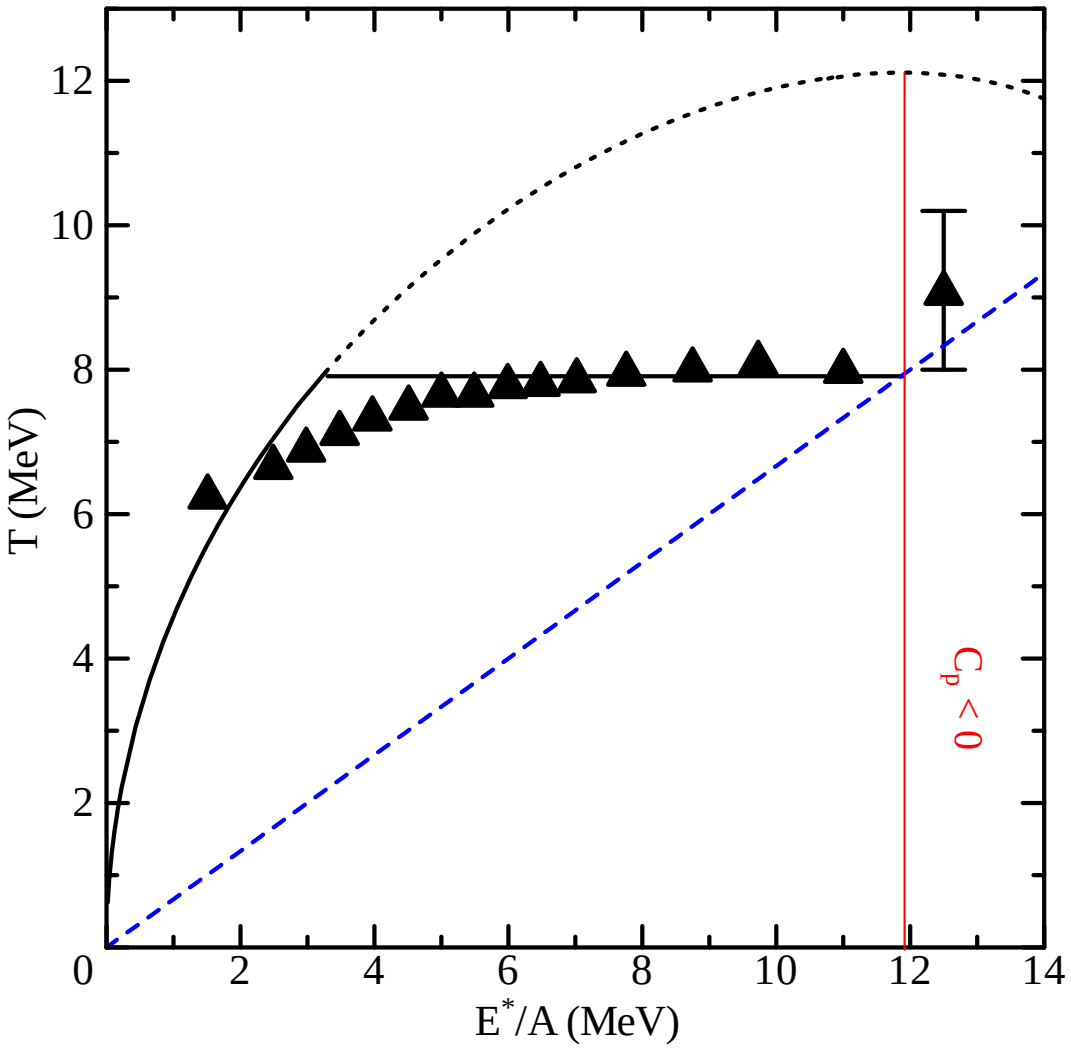

Figure 4: The black solid or dotted curve is the caloric curve corresponding to the black curve in Fig. 3. The horizontal black solid line is the boiling temperature of nuclear liquid, which corresponds to the common tangent in Fig. 3. The vertical red line shows the extreme of the temperature. The blue dashed line is the result $E^*/A = (3/2)\,T$ of a free gas. The triangles are the experimental data from Fig. 5 in Ref. [10].